Application of Direct Optimization Method by Zooms to Improve the Performances of AC Electromagnet

Alin-Iulian Dolan
University of Craiova, Faculty of Electrical Engineering, Craiova, Romania, adolan@elth.ucv.ro

***Abstract* – The paper seeks to improve the force developed by an AC electromagnet at maximum air-gap, using the direct optimization method by zooms, based on numerical experiments performed by finite element method (FEM) in ANSYS software. In a previous work, a 5.68% improvement in the static force characteristic of the same device was achieved and particularly, a 12.63% improvement in the force at maximum air-gap, taking into account three very influential geometrical parameters: the rate of bottom core thickness, rate of ring width and the rate of lateral core thickness. The optimization problem was subject to constraints of maintaining the overall dimensions of the device. The research continues in this paper with the search for the optimal geometrical configuration to provide a maximum developed force in the "open" position, replacing the parameter rate of ring width, having the least influence, with the parameter rate of winding thickness and adding the constraint of maintaining the cross-section of the winding. A device screening ensures that all the new three parameters are worth considering with a confidence level greater than 99%. The solution of the optimization problem brings an improvement of 25.67% of the acting force and of 7.09% of the static characteristic. The magnetic force was determined based on the principle of virtual work, available in ANSYS software.**

Cuvinte cheie: *optimizare, programarea experimentelor, metoda elementelor finite 2-D.*

Keywords: *optimization, DOE, 2-D FEM.*

I. Introduction

Numerical experiments remain the most effective tools to achieve fast and accurate results, especially in electromagnetism, where the finite element method (FEM) has become indispensable and many researchers have coupled it with design of experiments (DOE). Optimizing a device must be preceded by a screening to choose the most influential design variables. Of particular importance is the response surfaces methodology (RSM), providing useful information in running of optimization algorithms. Many papers present the use of these techniques to improve the performances of electromagnetic devices [1]-[14].

The RSM with FEM was used in [3] in order to optimize the performances of an electrical motor and in [4] to improve an electromagnet in magnetic levitation system based on many design variables.

The improvement of the static force characteristic of an electromagnetic actuator was often considered an appropriate case study to test different optimization methods.

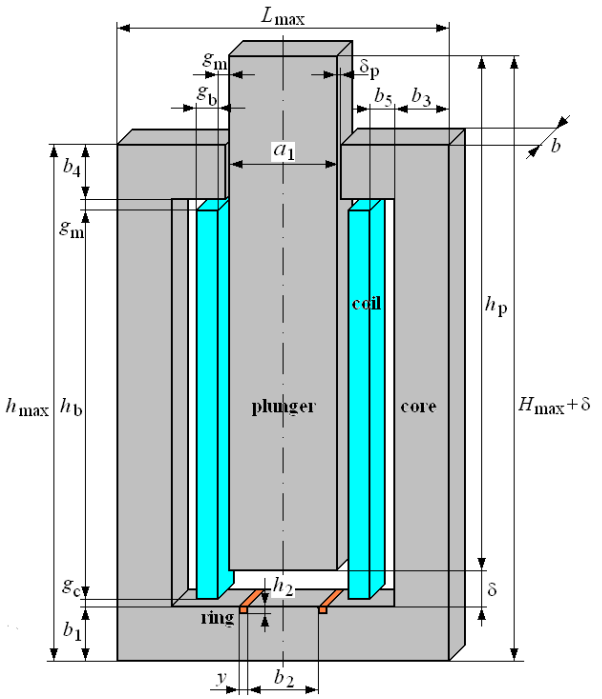

Fig. 1. Geometry of AC electromagnet [18].

The sequential quadratic programming (SQP) method was applied on a linear actuator after validation of a shape sensitivity analysis of magnetic forces using the Maxwell Stress Tensor approach and FEM [5]. The same tool allowed the force maximization of an electromagnet [6].

The sequential linear programming (SLP) method was applied in combination with 3-D FEM and RSM in order to optimize a permanent magnet linear actuator with moving magnet for driving a needle in a knitting machine [7]. The RSM was successfully used to maximize the clamping force of an electromagnetic linear actuator with divided coil excitation [9]. Also, an optimization strategy was performed on the average value of the electromagnetic force developed by an actuator [8].

In order to optimize the efficiency, specific power and cost of a tubular permanent magnet brushless linear motor with Halbach magnet array, the RSM was coupled with 2-D FEM, deducing mathematical relationships between input design variables and output performance.

A method for design optimization of permanent magnetic actuators for medium-voltage-class vacuum circuit breakers has given rise to scientific interest [11]. The RSM and FEM are used to minimize the weight of permanent magnet and to improve the dynamic characteristics.

The static magnetic force of a new type actuator for long stroke length with precise work performance is analyzed in [12] through ANSYS, ponting out several significant parameters affecting the dynamic characteristics and summarizing some general criteria for optimal design.

In [13] the FEM is applied for electromagnetic force computation for a solenoid type of electromagnetic actuator with ferrofluid. Influences of the various design parameters over the actuator characteristics are analysed and some of them are proposed to be used into optimization.

The paper [14] deals with the static characteristic analysis and force optimization of 3-DOF short-stroke planar motor, providing the basis and criterion for motor design.

Recent research on electromagnets has highlighted the effectiveness of the direct optimization method by zooms, based on the DOE technique coupled with FEM. Thus, in [16] and [18] the geometrical shapes of DC, respectively, AC electromagnets were optimized to maximize the static force characteristic using axisymmetric, respectively, planar models. In [17] the geometrical shape was obtained providing a maximum developed force at maximum air-gap (acting force) for the DC device.

The present study aims to maximize the acting force for AC electromagnet in [18] (Fig.1), while maintaining the overall dimensions: the width of the core (L_{max}), the height of the core (h_{max}) and the height of the plunger (H_{max}) and its winding cross section (S_b). The used optimization method by zooms is based on numerical experiments in ANSYS software, using planar model.

II. Screening of Device and Optimization Process

The initial geometric features of the device were calculated based on the design methodology in [15] (Table I [18]). Parameter b describes the depth of the magnetic core (Fig. 1 [18]).The electrical parameters are: the number of turns $N = 650$ with standard diameter $d = 0.8$ mm, the DC resistance $R_b = 6.086\ \Omega$, the rated supply voltage $U_r = 230$ V AC and the curve B-H of the core and the plunger is shown in Fig. 2. The range of the air gap is $\delta = [0.05 \div 10]$ mm.

Maximizing the static characteristic of [18] was performed under the same conditions, taking into account the variation of three parameters: the rate of bottom core thickness k_1, the rate of ring width k_2 and the rate of lateral core thickness k_3:

$$k_1 = \frac{b_1}{a_0} \in [0.8 \div 1.2] \tag{1}$$

$$k_2 = \frac{b_2}{a_2} \in [0.8 \div 1.2] \tag{2}$$

$$k_3 = \frac{b_3}{a_0} \in [0.8 \div 1.2] \tag{3}$$

The influence of the three parameters on the static force characteristic was certified by the screening of device with respect to response function Y which takes into account 4 values of force at 4 air-gaps $\delta = 0.05, 0.2, 2, 10$ mm:

$$Y = \sqrt{\frac{c}{4} \cdot \sum_{k=1}^{4} \left(\frac{F_k - F_0}{F_0} \right)^2} \tag{4}$$

TABLE I.
Geometrical Parameters of AC Electromagnet [18]

a_0 (mm)	15.356	g_{b0} (mm)	5.968
a_1 (mm)	30.712	S_b (mm^2)	657.501
a_2 (mm)	20.475	g_c (mm)	2.000
b (mm)	44.226	g_m (mm)	3.000
b_1 (mm)	15.356	h_2 (mm)	1.589
b_2 (mm)	20.475	y (mm)	2.000
b_3 (mm)	15.356	L_{max} (mm)	93.361
b_4 (mm)	15.356	h_{max} (mm)	145.884
b_5 (mm)	7.000	H_{max} (mm)	161.240
δ_p (mm)	1.000		

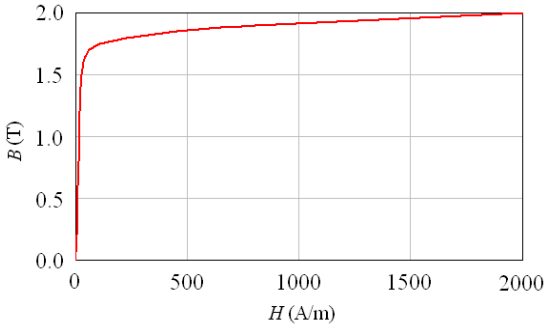

Fig. 2. The B-H curve for plunger and core [18].

where $F_0 = 1500$ N and $c = 100$ are reference values.

The Table II includes the quantiles F_{obs} of the Fisher-Snedecor observed value with 1 and 4 degrees of freedom, the corresponding effects and probabilities $P(F \le F_{obs})$.

The histogram of the effects (Fig. 3) shows that for the confidence level $1 - \alpha = 99\%$, all three parameters have a significant influence on the static characteristic: $P_1 = 99.983\%$, $P_2 = 99.998\%$ and $P_3 = 99.972\%$.

Maximizing of static force characteristic means minimizing of response Y, imposing gauge constraints:

$$\mathrm{P}: \begin{cases} \min Y(k_1, k_2, k_3, b_4, b_5, h_p) \\ 0.8 \le k_1 \le 1.2 \\ 0.8 \le k_2 \le 1.2 \\ 0.8 \le k_3 \le 1.2 \\ g_L(k_1, k_2, k_3) = 0 \\ g_h(k_1, k_2, k_3) = 0 \\ g_H(k_1, k_2, k_3) = 0 \end{cases} \tag{5}$$

$$g_L(k_1, k_2, k_3) = a_1 + 2 \cdot (g_c + g_m + g_b + b_5 + k_3 \cdot a_0) - L_{max} \tag{6}$$

$$g_h(k_1, k_2, k_3) = b_4 + h_b + a_0 \cdot k_1 - h_{max} \tag{7}$$

$$g_H(k_1, k_2, k_3) = h_p + a_0 \cdot k_1 - H_{max} \tag{8}$$

The direct optimization method by zooms is fully described in [2] and consists of the iteratively realization of a full factorial design counting $2^3 + 1 = 9$ numerical experiments corresponding to the vertices and to the center of a 3-D hyper-rectangle.

The point with better response is selected as the center of the next 3-D area with equal or lower volume.

Applying the described method, after 4 iterations was obtained the optimal solution $k_1 = 1.2$, $k_2 = 1.1$, $k_3 = 0.8$, corresponding to the best response $Y = 7.483$ with the

TABLE II.
RESULTS OF SCREENING FOR STATIC CHARACTERISTIC [18]

Source of variation	$F_{obs}(m)$	Effects $E(x_m)$	Probability $P_m = 1 - \alpha_m$
k_1	186.976	-0.02843	0.99983
k_2	576.809	-0.04994	0.99998
k_3	143.539	0.02491	0.99972
$k_1 \cdot k_2$	0.076	0.00057	0.20308
$k_1 \cdot k_3$	3.419	-0.00385	0.86187
$k_2 \cdot k_3$	0.503	0.00147	0.48254
$k_1 \cdot k_2 \cdot k_3$	0.002	0.00010	0.03654
Total	F_{obs}_99% = 21.198, E_99% = 0.00957		

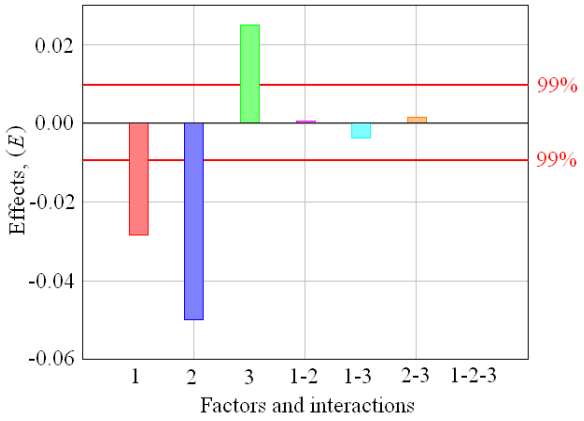

Fig.3. The histogram of effects for static characteristic [18].

error ε_Y = -0.03%. The graphical illustration of the optimization algorithm is shown in Fig. 4 and Fig. 5 [18].

Parameter k_2 reached the optimal value inside its variation range and the others k_1 and k_2, on the borders. A total of 180 numerical experiments were performed to improve the performance of the device by 5.68%. Particularly, the force developed at maximum air gap had an increase of 12.63%. Other dimensions were done in Table III [18].

The device research continues in this paper with the search for an optimal geometrical configuration to provide a maximum attraction force in the "open" position. Since the influence of the ring is very low at air gap values greater than 1 mm, the study considers another geometrical parameter k_4 related to the winding thickness of the electromagnet, under constraint of maintaining its cross section S_b:

$$k_4 = \frac{g_b}{g_{b0}} \in [1.0 \div 1.2] \qquad (9)$$

The results of a new screening based on 4 parameters are shown in Table IV. The histogram of effects (Fig. 6) shows that the parameter k_2 can be rejected with the risk of 6.232%, which was expected.

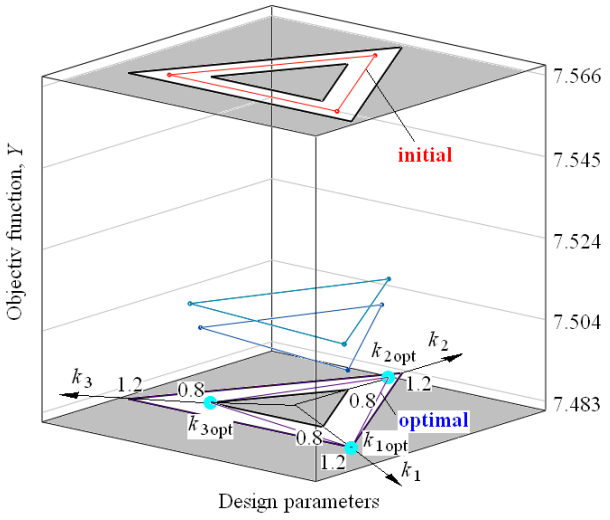

Fig. 4. The 3-D feasible domain (white surface on gray planes) and the evolution of design parameters during optimization algorithm for static force characteristic [18].

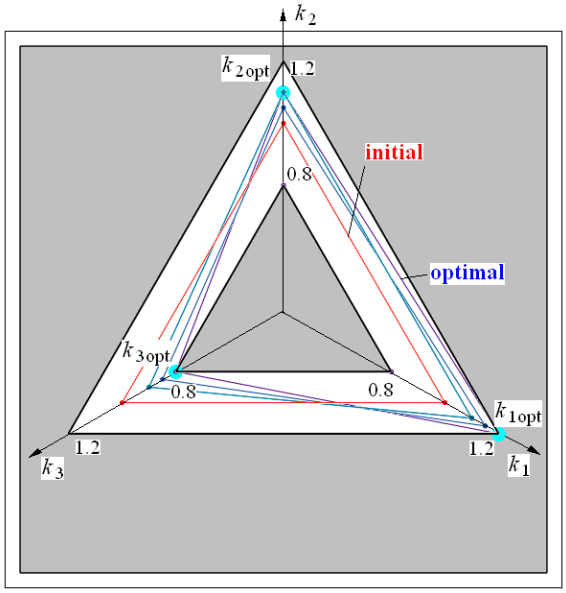

Fig. 5. The 3-D feasible domain (white surface on gray planes) and the evolution of design parameters during optimization algorithm for static force characteristic (2-D view) [18].

The rest of the parameters k_1, k_3, k_4, for confidence level 1 - α = 99%, are considered very influential on the acting force, with the probabilities P_1 = 99.973%, P_3 = 99.999%, respectively, P_4 = 99.999%.

TABLE III.
ITERATIONS OF OPTIMIZATION ALGORITHM FOR STATIC FORCE CHARACTERISTIC [18]

Iterations	N_{tot}	N_{rec}	k_1	k_2	k_3	Y	ε_Y (%)	b_1 (mm)	b_2 (mm)	b_3 (mm)	b_4 (mm)	h_p (mm)
0	-	-	1.00	1.00	1.00	7.566	-	15.36	20.47	15.36	15.36	145.88
1	9	4	1.10	1.10	0.90	7.508	-0.77	16.89	22.52	13.82	13.82	144.35
2	9	2	1.10	1.10	0.90	7.508	0.00	16.89	22.52	13.82	13.82	144.35
3	9	1	1.15	1.05	0.85	7.502	-0.08	17.66	21.50	13.05	13.05	143.58
4	9	0	**1.20**	**1.10**	**0.80**	**7.483**	**-0.25**	**18.43**	**22.52**	**13.82**	**12.28**	**142.81**
TOTAL	**36**	**7**										

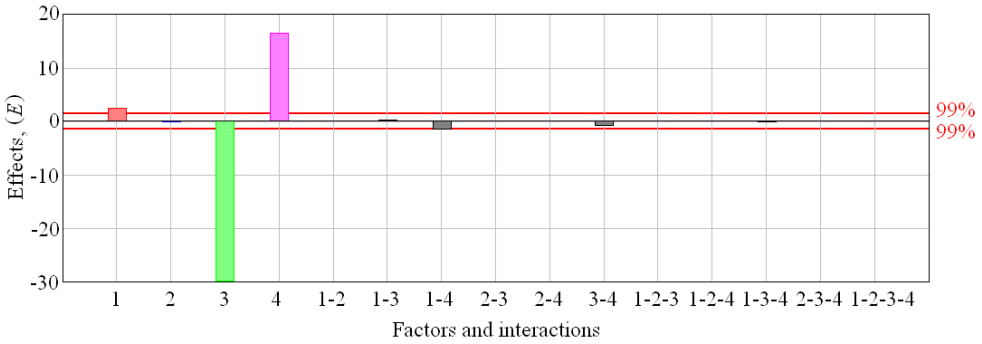

Fig. 6. Histogram of effects for acting force.

TABLE IV.
RESULTS OF SCREENING FOR ACTING FORCE

Source of variation	$F_{obs}(m)$	Effects $E(x_m)$	Probability $P_m = 1 - \alpha_m$
k_1	27.809	2.513	0.99973
k_2	0.006	-0.038	0.06232
k_3	3915.908	-29.822	0.99999
k_4	1184.901	16.404	0.99999
$k_1 \cdot k_2$	0.000	-0.001	0.00102
$k_1 \cdot k_3$	0.103	0.153	0.24600
$k_1 \cdot k_4$	8.332	-1.376	0.98520
$k_2 \cdot k_3$	0.001	0.012	0.01943
$k_2 \cdot k_4$	0.000	-0.007	0.01125
$k_3 \cdot k_4$	2.647	-0.761	0.86122
$k_1 \cdot k_2 \cdot k_3$	0.000	-0.001	0.00102
$k_1 \cdot k_2 \cdot k_4$	0.000	0.001	0.00102
$k_1 \cdot k_3 \cdot k_4$	0.016	-0.061	0.09893
$k_2 \cdot k_3 \cdot k_4$	0.000	0.003	0.00511
$k_1 \cdot k_2 \cdot k_3 \cdot k_4$	0.000	0.001	0.00102
Total	$F_{obs}\_99\% = 9.646$, $E\_99\% = 1.480$		

Therefore, the new optimization problem also depends on 3 parameters (k_1, k_3, k_4), plus the constraint that preserves the winding cross section S_b. The parameter k_2 is initialized to 1.1, representing its optimal value computed in [18]. The equations describing the optimization problem are the following:

$$\mathrm{P}:\begin{cases} \max F_a(k_1,k_2,k_3,k_4,b_4,b_5,h_p,h_b) \\ 0.8 \le k_1 \le 1.2 \\ k_2 = 1.1 \\ 0.8 \le k_3 \le 1.2 \\ 1.0 \le k_4 \le 1.2 \\ g_L(k_3,k_4,b_5) = 0 \\ g_h(k_1,k_4,h_b) = 0 \\ g_H(k_1,h_p) = 0 \\ g_{Sb}(k_4,h_b) = 0 \end{cases} \quad (10)$$

$$g_L(k_3,k_4,b_5) = a_1 + 2\cdot(g_c + g_m + g_{b0}\cdot k_4 + b_5 + k_3\cdot a_0) - L_{max} \quad (11)$$

$$g_h(k_1,k_4,h_b) = b_4 + h_b + a_0\cdot k_1 - h_{max} \quad (12)$$

$$g_H(k_1,h_p) = h_p + a_0\cdot k_1 - H_{max} \quad (13)$$

$$g_{Sb}(k_4,h_b) = h_b\cdot g_{b0}\cdot k_4 - S_b \quad (14)$$

Applying the direct optimization method by zooms, the optimal solution $k_1 = 1.2$, $k_3 = 0.8$, $k_4 = 1.2$, corresponding to the biggest acting force $F_a = 303.23$ N, was obtained after 4 iterations, with the $\varepsilon_{Fa} = 0.00\%$ error. The graphic illustration of the optimization algorithm is shown in Fig. 7 and Fig. 8.

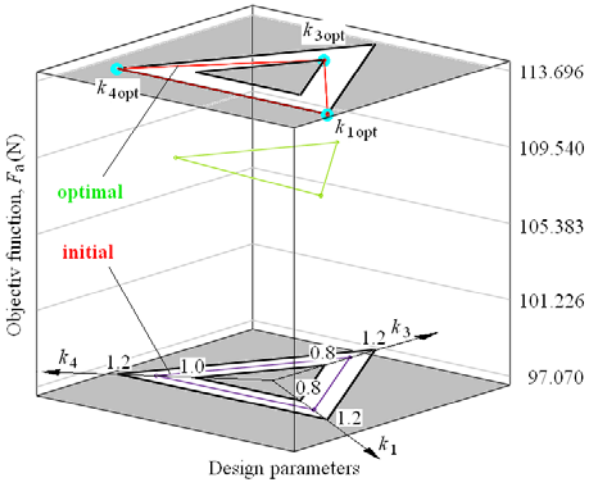

Fig. 7. The 3-D feasible domain (white surface on gray planes) and the evolution of design parameters during optimization algorithm for acting force.

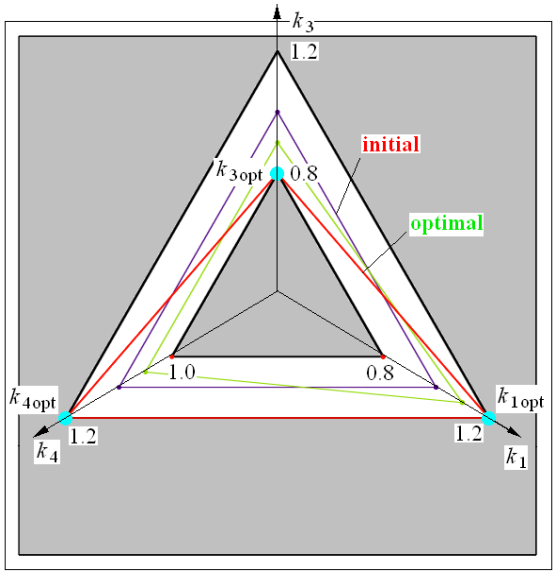

Fig. 8. The 3-D feasible domain (white surface on gray planes) and the evolution of design parameters during optimization algorithm for acting force (2-D view) [18].

The parameters k_1, k_3, k_4 have reached the optimal values on the borders of the variation range. A total of 50 numerical experiments were performed resulting an improvement of the acting force by 25.67%. In Table V the other geometric dimensions were calculated.

The numerical simulations were performed with ANSYS software using command files written in APDL language. The 2-D planar solution takes into account the depth b of the device (Fig.1). For harmonic analyses the frequency of 50 Hz was considered. The magnetic force was computed using the Virtual Work principle.

The Fig. 9 presents comparatively the distribution of real and imaginary components of magnetic flux density for the initial configuration (left) [15] and for the configuration corresponding to the optimal static characteristic (right) at δ = 10 mm computed in [18]. The design methodology in [15] takes into account the approximate analytical formula for permeances.

The Fig. 10 presents the same components to compare the initial configuration (left) and the configuration corresponding to the optimal acting force (right) at δ = 10 mm.

The acting force corresponding to the optimal configuration can be seen in Fig. 11, on the static characteristic. Here is also added the static force characteristic analytically and numerically calculated by the design methodology [15] and the one optimized according to the parameters k_1, k_2, k_3 [18]. The analytical evaluation of the force is based on the approximation of magnetic flux lines through straight lines and arcs [15].

It can be noticed that besides the improvement of the acting force from 12.63% [18] to 25.67%, an improvement of the static characteristic was obtained from 5.68%

TABLE V.
ITERATIONS OF OPTIMIZATION ALGORITHM FOR ACTING FORCE

Iterations	N_{tot}	N_{rec}	k_1	k_2	k_3	k_4	F_a (N)	ε_{Fa} (%)	b_1 (mm)	b_2 (mm)	b_3 (mm)	b_4 (mm)	h_p (mm)	g_b (mm)
0	-	-	1.00	1.10	1.00	1.10	256.22	-	15.36	22.52	15.36	25.37	145.88	6.56
1	9	0	1.10	1.10	0.90	1.20	289.93	13.16	16.89	22.52	13.82	32.18	144.35	7.16
2	9	0	1.20	1.10	0.80	1.20	303.23	4.58	18.43	22.52	12.28	30.65	142.81	7.16
3	9	1	1.20	1.10	0.80	1.20	303.23	0.00	18.43	22.52	12.28	30.65	142.81	7.16
4	9	1	**1.20**	**1.10**	**0.80**	**1.20**	**303.23**	**0.00**	**18.43**	**22.52**	**12.28**	**30.65**	**142.81**	**7.16**
Total	**36**	**2**												

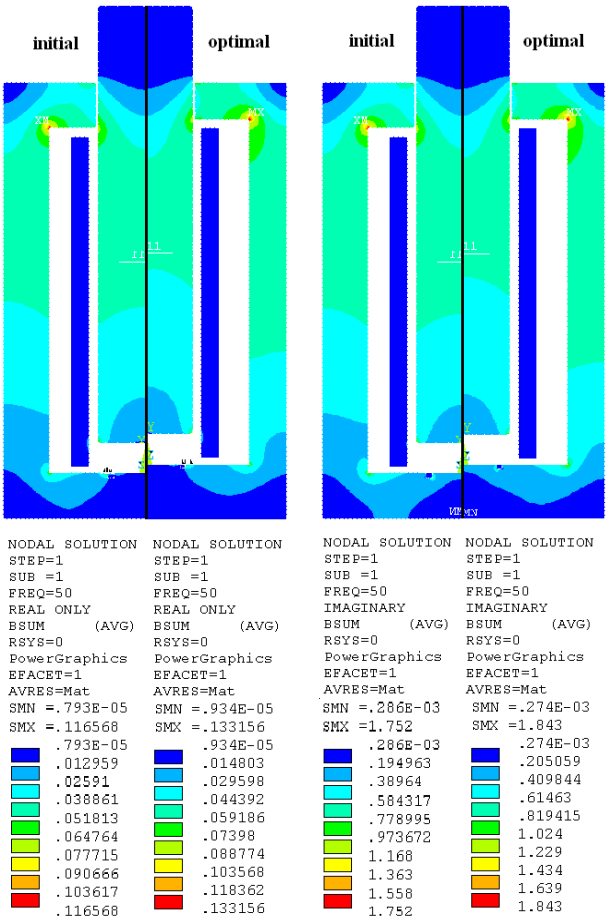

Fig. 9. Real and imaginary components of magnetic flux density for the initial configuration (left) and for configuration corresponding to optimal static characteristic (right) at δ = 10 mm (ANSYS, planar solution) [18].

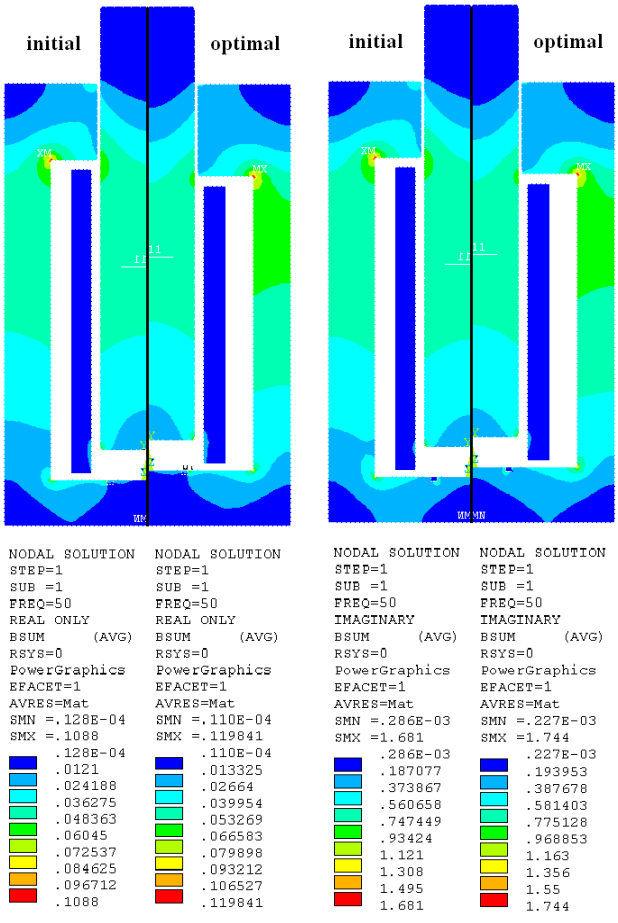

Fig. 10. Real and imaginary components of magnetic flux density for the initial configuration (left) and for configuration corresponding to the optimal acting force (right) at δ = 10 mm (ANSYS, planar solution).

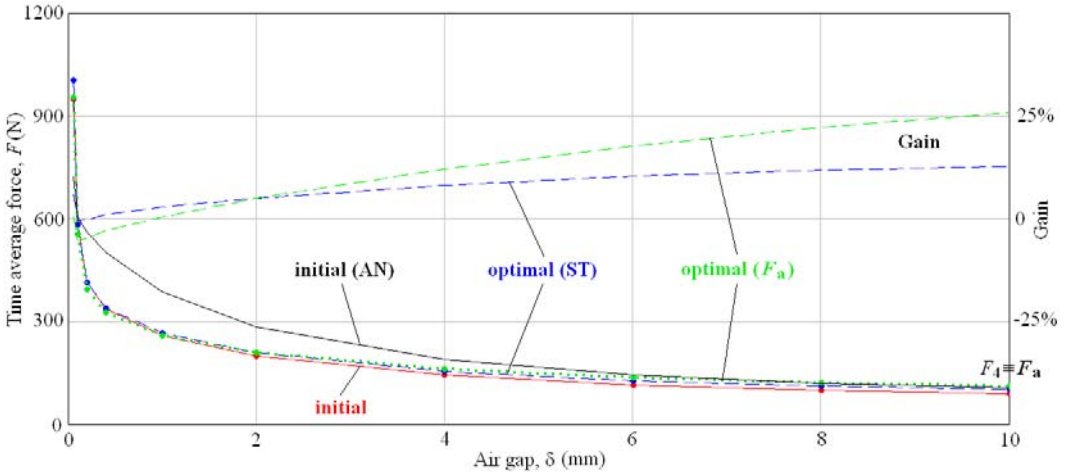

Fig. 11. Optimal numerical results for static force characteristic and acting force compared to analytical and numerical results of initial configuration.

[18] to 7.09%, which shows the strong influence of parameter k_4. Taking into account k_4 and [18] could lead to superior performance.

The improvement of 7.09% of static characteristic includes the range of the air-gap $\delta = [0.05 \div 0.9]$ mm, where lower forces were obtained, compared to characteristic numerically computed by [15].

III. Conclusions

Using the direct optimization method by zooms and the FEM 2-D, the performance of an AC electromagnet in terms of acting force was improved.

The optimization problem takes into account three geometrical parameters with very strong influence: the rate of the bottom core thickness, the rate of ring width, the rate of lateral core thickness and the rate of winding thickness having as constraints the maintaining of the overall dimensions and the cross-section of the winding.

The solution brings an improvement of 25.67% of the acting force and of 7.09% of the static force characteristic.

Acknowledgment

Source of research funding in this article: Research program of the Electrical Engineering Department financed by the University of Craiova.

Contribution of authors:

First author – 100%

Received on July 17, 2018

Editorial Approval on November 15, 2018

References

[1] D. Montgomery, Design and analysis of experiment, 5-th Edition, Arizona State University, 2000.

[2] S. Vivier, "Strategies d'optimisation par la methode des plans d'experiences et applications aux dispositives electrotechniques modelise par elements finis," Ph-D Thesis, Lille, 2002.

[3] F. Gillon, and P. Brochet, "Screening and response surface method applied to the numerical optimization of electromagnetic devices," IEEE Trans. on Magnetics, Vol. 36, No. 4, pp.1163-1166, 2000.

[4] D.-K. Hong, K.-C. Lee, B.-C. Woo, and D.-H. Koo, "Optimum design of electromagnet in magnetic levitation system for contactless delivery application using response surface methodology," Proceedings of the 2008 Int. Conf. on El. Machines, pp. 1-6, 2008.

[5] J.-M. Biedinger, and D. Lemoine, "Shape sensitivity analysis of magnetic forces", IEEE Transactions on Magnetics, Vol. 30, pp. 2309-2516, 1997.

[6] G. Sefkat, "The design optimization of the electromechanical actuator," Structural and Multidisciplinary Optimization, February 2009, Volume 37, Issue 6, pp. 635–644, 2009.

[7] I. Yatchev, M. Rudnicki, K. Hinov, and V. Gueorgiev, "Optimization of a permanent magnet needle actuator," COMPEL, Vol. 31, Issue 3, pp. 1018-1028, 2012.

[8] S. Yong, J. Tong, S. Enze, and Y. Zaiming, "Analysis and optimization of static characteristics in overall operating conditions of electromagnetic actuator," Research Journal of Applied Sciences, Engineering and Technology 7(8), pp. 1561-1567, 2014.

[9] T.-W. Kim, and J.-H. Chang, "Optimal design of electromagnetic actuator with divided coil excitation to increase clamping force," Journal of International Conference on Electrical Machines and Systems, pp. 1461-1464, 2014.

[10] K. Li, X. Zhang, and H. Chen, "Design Optimization of a Tubular Permanent Magnet Machine for Cryocoolers", IEEE Transactions on Magnetics, Vol. 51, pp.1-8, 2015.

[11] H.-M. Ahn, T.-K. Chung, Y.-H. Oh, K.-D. Song, Y.-I. Kim, H.-R. Kho, M.-S. Choi, and S.-C. Hahn, "Optimal Design of Permanent Magnetic Actuator for Permanent Magnet Reduction and Dynamic Characteristic Improvement using Response Surface Methodology," J. Electr. Eng. Technol.2015, 10(3): pp. 935-943, 2015.

[12] E. Dong, Z. Zhang, H. Dong, and C. Fang, "The dynamic characteristic simulation and finite element method analysis of magnetic force actuator for long stroke length high voltage circuit breaker," IV-th IEEE Int. Conf. on El. Utility Deregulation and Restructuring and Power Technologies (DRPT), pp. 1590-1593, 2011.

[13] V. Mateev, A. Terzova, and I. Marinova, "Design Analysis of Electromagnetic Actuator with Ferrofluid," XVIII-th IEEE International Symposium on Electrical Apparatus and Technologies (SIELA 2014), May 29-31, pp. 1-4, 2014.

[14] He Zhang, B. Kou, Hailin Zhang, and Y. Jin, "Static Characteristic Analysis and Force Optimization of a Short-Stroke Planar Motor," XIX-th International Conference on Electrical Machines and Systems (ICEMS), November 13-16, pp. 1-5, 2016.

[15] G. Hortopan, Electrical apparatus of low voltage (in Romanian), Tehnica Publishing House, Bucharest, 1969.

[16] A.-I. Dolan, "Optimization of DC electromagnet using design of experiments and FEM," XIII-th IEEE International Conference on Applied and Theoretical Electricity – ICATE 2016, Craiova, Romania, October 06-08, pp. 1-6, 2016.

[17] A.-I. Dolan, "Optimal shape of DC electromagnet," Annals of the University of Craiova, Series: Electrical Engineering, No. 40, pp. 9-13, Universitaria Publishing House, 2017.

[18] A.-I. Dolan, "Improvement of static force characteristic of AC electromagnet using DOE and FEM," XIV-th IEEE International Conference on Applied and Theoretical Electricity – ICATE 2018, Craiova, Romania, October 03-05, pp. 1-5, 2018.